

glass in samples MA90-7, MA90-20, and MA90-23 contained significant feldspar microlites. To insure that only pure glass (>99%) was analyzed, a special procedure was developed to separate even finely disseminated impurities from the glass. The final purity was determined by the inspection of powdered bulk glass separates (<325 mesh; 45 μm) with transmitted light microscopy and by comparison of the DCP bulk glass Fe, Ca, Al, Mn, and Ti concentrations with those determined by grain discrete electron microprobe analyses. These steps were applied to all samples of this study to facilitate comparisons and correlations. Concentrations of Fe, Ca, Al, Mn, and Ti were determined by comparison of unknown intensities to calibration curves on the basis of six internationally recognized rock standards. All other concentrations were determined by the method of standards addition with the use of a multi-element spike solution designed specifically for silicic compositions.

33. The Ca/K ratio is derived by the multiplication of the measured $^{37}\text{Ar}/^{39}\text{Ar}$ ratio by 1.96. The weighted mean age and error (\pm 1 sigma) are computed

with an inverse variance weighting factor that uses deviations about a weighted mean to determine the weighted error (30, 31). Individual grain errors reflect errors in the fluence monitor constant (J) and in the determination of Ar isotopic ratios, which in turn propagate errors in discrimination and in Ar beam intensities from sample and blank (30). The data in italics are excluded from the mean age. Feldspars were irradiated for 0.5 hour at 8 MW at the Omega West research reactor of the Los Alamos National Laboratory, which has a fast neutron fluence of 5.7×10^{13} neutrons per centimeter per second. Cadmium shielding was used to reduce the thermal neutron production of ^{40}Ar . After irradiation, the samples were transferred to a copper holder and loaded onto the extraction line for overnight bakeout at $\sim 200^\circ\text{C}$. Samples were fused with an 8-W argon-ion laser (Mass Analyser Products, Nottingham, United Kingdom). Abundances of the argon isotopes were measured on a MAP-215 noble gas spectrometer fitted with a Balzers electron multiplier operating at a gain of about 20,000. Typical

system blank volumes of ^{40}Ar , ^{39}Ar , ^{38}Ar , ^{37}Ar , and ^{36}Ar are 4, 2, 0.08, 0.3, and 0.3×10^{-17} mol, respectively. Sanidine from the Fish Canyon tuff was used as the neutron fluence monitor, which has a reference age of 27.84 Ma (30). The constants used in this study are as follows: $(\lambda_e + \lambda_c) = 0.581 \times 10^{-10}$ /year; $\lambda_\beta = 4.962 \times 10^{10}$ /year; 40 K per degree kelvin = 1.167×10^{-4} mol/mol).

34. We thank the National Science Foundation, the National Geographic Society, the Japan Society for the Promotion of Science, the University of California Collaborative Research Program of the Institute of Geophysics and Planetary Physics at Los Alamos National Laboratory, the Ethiopian Ministry of Culture and Sports Affairs, the National Museum of Ethiopia, the Afar people, A. Ade-massu, B. Latimer, S. Yirga, G. Hundie, A. Negash, Z. Assefa, and C. Tilahun for making the 1990 Middle Awash research possible. We also thank F. C. Howell and B. Dalrymple for helpful suggestions on the paper.

8 February 1994; accepted 2 May 1994

MCM-22: A Molecular Sieve with Two Independent Multidimensional Channel Systems

Michael E. Leonowicz, Jeffrey A. Lawton,* Stephen L. Lawton,†
Mae K. Rubin

The molecular sieve MCM-22 contains structural features previously unobserved in this class of materials. Its framework topology, derived from high-resolution electron micrographs and refined with synchrotron x-ray diffraction powder data, contains two independent pore systems, both of which are accessed through rings composed of ten tetrahedral (T) atoms (such as Si, Al, and B). One of these pore systems is defined by two-dimensional, sinusoidal channels. The other consists of large supercages whose inner free diameter, 7.1 angstroms, is defined by 12 T-O species (12-rings) and whose inner height is 18.2 angstroms. These coexisting pore systems may provide opportunities for a wide variety of catalytic applications in the petrochemical and refining industries. Another structural feature is an unusual -T-O-T- chain that passes through the center of a modified dodecasil-1H [$4^35^66^3$] cage.

Molecular sieves are crystalline, microporous materials with frameworks of tetrahedral atoms that are interconnected in three dimensions through oxygen atoms. Their pore structure makes them useful in the petrochemical and refining industries for catalysis and separation processes. Synthesis is usually carried out under hydrothermal conditions. A directing agent, if present in the reaction gel, may be used to influence the formation and geometry of the internal pore system. The molecular sieve MCM-22 was synthesized in this manner, with hexahydro-1H-azepine (hexamethyleneimine) as a directing agent. We propose a model for the structure of this molecular sieve.

MCM-22 may be synthesized as an aluminosilicate or borosilicate. Scanning electron micrographs revealed that it crystallizes as

very thin sheets and that boron MCM-22 crystallites are typically thicker than those from aluminum syntheses. Boron-containing samples were chosen for structural studies because their large size gave rise to powder x-ray diffraction (XRD) patterns with sharper peaks.

The MCM-22 sample used in this study was hydrothermally synthesized by procedures described elsewhere (1) from Hi-Sil precipitated silica (87% SiO_2), hexamethyleneimine (HMI), triethanolamine, boric acid (H_3BO_3), and sodium hydroxide (50% NaOH solution). Triethanolamine (320 g) was added to a solution containing 14.0 g of H_3BO_3 , 6.3 g of NaOH, and 160 g of H_2O ; 96.0 g of Hi-Sil were then added, followed by 42.0 g of HMI. After vigorous stirring for 1 hour, 100 g of this slurry were transferred to a Teflon-lined stainless steel autoclave. The vessel was placed in an oil bath, and the reaction mixture was crystallized under static conditions at 120°C for 230 days. The solid product was washed with water and dried overnight at 120°C (2) and then

calcined in air at 540°C for 16 hours. This calcined product, $\text{H}_{0.033}\text{Na}_{0.043}(\text{Al}_{0.005}\text{B}_{0.071}\text{Si}_{0.924})\text{O}_2$, is referred to as MCM-22.

Electron diffraction (ED) photographs indicated that the unit cell had hexagonal symmetry with no systematic absences. They exhibited Laue symmetry consistent with the eight hexagonal space groups $P6/mmm$, $P62m$, $P6m2$, $P6mm$, $P622$, $P31m$, $P31m$, and $P312$. The XRD data for the structure refinement of the calcined sample were collected on beamline X7A at the National Synchrotron Light Source in Brookhaven National Laboratory (3). These data were successfully indexed on a hexagonal lattice and were fully consistent with a space group that exhibits no systematic extinctions. The refined unit cell parameters were $a = 14.1145(8)$ Å and $c = 24.8822(18)$ Å (4).

The structure was determined with high-resolution electron micrograph (HREM) lattice images and model building. Trial models were refined by the program DLS (5), and the model whose calculated XRD pattern most closely resembled the experimental pattern was subjected to a Rietveld refinement (6) (Fig. 1). Final atomic coordinates are given in Table 1. There are 72 T atoms per unit cell.

As seen in projections of the framework topology for MCM-22 (Figs. 2 and 3), the [001] projection is remarkably similar to that of the silica clathrate dodecasil-1H (DOH) (7) (Fig. 3). Topologically, the two framework connectivities are related. The DOH structure contains hexagonal sheets of [$4^35^66^3$] cages (8) (Fig. 4A) that share 4-ring faces with adjacent cages within the sheet. Large 12-ring cavities bordered by six joined cages are created within these sheets. These sheets, in turn, join along the unit cell c direction through single 6-rings that cap the 12-ring cavities at either end, giving the cavity [6^85^{12}] topology. Adjacent sheets are also directly connected through bonds between apical T atoms on the threefold axes of [$4^35^66^3$] cages.

Mobil Research and Development Corporation, P.O. Box 480, Paulsboro, NJ 08066, USA.

*Present address: Program in Cell and Molecular Biology, Baylor College of Medicine, One Baylor Plaza, Houston, TX 77030, USA.

†To whom correspondence should be addressed.

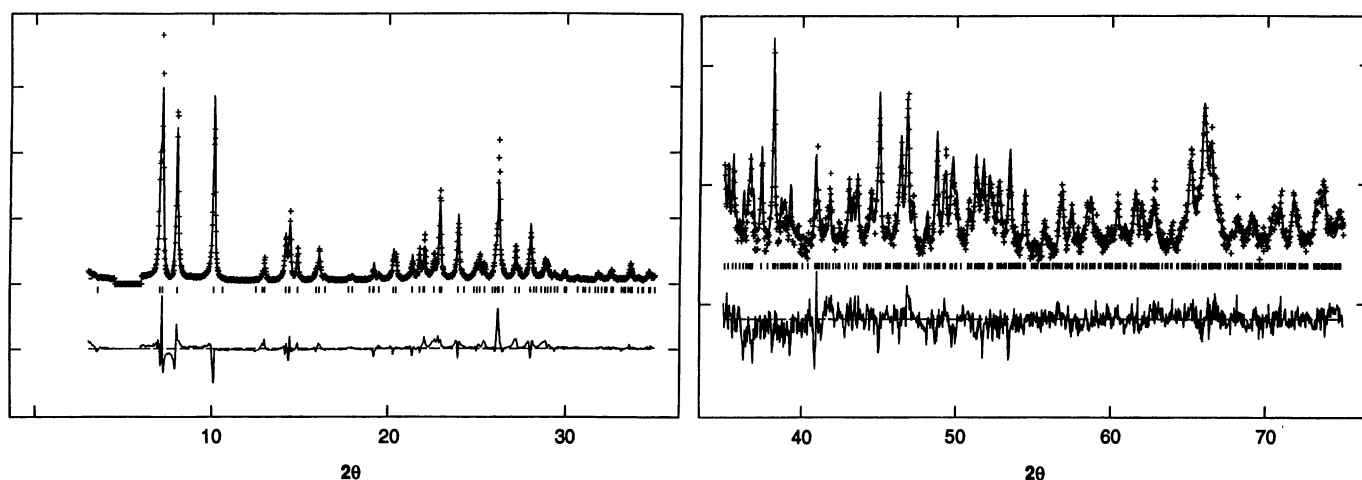


Fig. 1. Observed (+) and calculated (solid line) powder patterns and the difference (lower line) profile for the Rietveld refinement of MCM-22.

In MCM-22, the DOH $[4^35^66^3]$ cage is modified: The orientation of the two apical T atoms on the threefold axis is reversed, and these atoms join inside the cage through a shared oxygen atom. This unusual coordination inside the cage is completed by the placement of a TO_3 cap on top of the cage, forming a small $[4^3]$ unit (Fig. 4B). (This small unit has previously been found in the three zeolites that form the natrolite group: edingtonite, natrolite, and thomsonite.) The T atom located at the top of the $[4^3]$ unit serves as the link that joins two identical layers together through a shared oxygen atom. This linkage forms slightly elliptical 10-ring apertures to large supercages having $[4^25^810^2]$ topology and inside free dimensions of 7.1 Å by 7.1 Å by 18.2 Å. The supercages stack one above the other through double 6-rings, an arrangement that forms two-dimensional, sinusoidal, intralayer channels with access through elliptical, slightly folded 10-ring apertures. The diameter of the supercage is defined by 12-rings. The top and bottom halves of the supercage define surface pockets in the layer that resemble DOH $[6^85^{12}]$ cavities with the 6-ring cap removed from one end. There is no communication between the interlayer supercage and the intralayer sinusoidal channel.

Although the average, weighted bond length (1.61 Å) and nonsymmetry-constrained T-O-T angles (136° to 164°) of the refined model are reasonable for silicate framework structures, there is considerable variation from idealized values in individual cases. The geometry about atoms associated with the crystallographic threefold axis of the $\{4^35^66^3[4^3]\}$ cage is distorted. The bond length of the oxygen bridge between the layers, T1-O1, is 1.45(3) Å, and the bond lengths of the T-O-T connectivity through the capped $\{4^35^66^3[4^3]\}$ cage are T4-O5 = 1.52 Å and T5-O5 = 1.72 Å. The refined model also has an unusually long [1.71(3) Å] T2-O4 bond

within the $[4^3]$ cap, and a short [1.49(4) Å] T8-O11 bond between the double 6-ring and the $\{4^35^66^3[4^3]\}$ cage. These deviations may be artifacts of the least squares minimization process in the $P6/mmm$ space group. All other bond lengths are within 2σ of 1.61 Å.

Resident within the framework is a T-O- $[4^3]$ -O- $[4^3]$ -O-T chain parallel with the unit cell c axis (Fig. 5). The T-O- $[4^3]$ - segment is part of the $\{4^35^66^3[4^3]\}$ cage, and the central oxygen atom in the $-[4^3]$ -O- $[4^3]$ - segment is

the bridge that links two MCM-22 layers together. Within this chain, T-O-T angles involving atoms that are situated on the threefold axis (namely, T1-O1-T1 and T4-O5-T5) are constrained to be linear in space group $P6/mmm$. Because stereochemical bonding considerations predict that T-O-T bonds are not linear in their local environments, the crystallographic space group $P6/mmm$ probably represents only an average symmetry for the MCM-22 framework. Con-

Table 1. Fractional atomic coordinates for boron MCM-22 [space group $P6/mmm$ (no. 191), $a = 14.1145(8)$ Å, $c = 24.8822(18)$ Å]. Numbers in parentheses are the estimated standard deviations (SDs) in the least significant digit. Parameters without estimated SDs were held fixed in the least squares refinement. Thermal parameters for the framework atoms (T and O) and for the nonframework atoms (S) were constrained to $U = 0.013, 0.025, \text{ and } 0.040$ Å², respectively. Framework atoms have full occupancy; nonframework atoms, defined as neutral oxygen, have the following refined occupancies: S1, 0.92(12); S2, 0.50(6); S3, 0.54(3); S4, 0.68(6); and S5, 0.85(4).

Atom	Position*	x	y	z
T1	4h	0.6667	0.3333	0.0581(11)
T2	12o	0.4662(13)	0.2331(7)	0.1347(7)
T3	12n	0.3850(12)	0.0	0.1646(7)
T4	4h	0.6667	0.3333	0.2124(12)
T5	4h	0.6667	0.3333	0.3428(12)
T6	12n	0.3869(12)	0.0	0.2891(7)
T7	12o	0.4192(13)	0.2096(6)	0.3480(7)
T8	12o	0.2574(13)	0.1287(6)	0.4375(7)
O1	2c	0.6667	0.3333	0.0
O2	12o	0.5408(12)	0.2704(6)	0.0791(11)
O3	24r	0.3873(14)	0.0998(11)	0.1346(9)
O4	12o	0.5472(14)	0.2736(7)	0.1906(11)
O5	4h	0.6667	0.3333	0.2735(15)
O6	12n	0.3710(23)	0.0	0.2269(11)
O7	6i	0.5	0.0	0.1527(19)
O8	6i	0.5	0.0	0.3056(18)
O9	24r	0.3832(16)	0.1004(12)	0.3135(8)
O10	12o	0.5448(13)	0.2724(6)	0.3656(12)
O11	12o	0.3550(23)	0.1775(12)	0.4018(12)
O12	12n	0.1784(19)	0.0	0.4205(13)
O13	6m	0.3022(32)	0.1511(16)	0.5
S1	3f	0.5	0.0	0.0
S2	6j	0.409(9)	0.0	0.0
S3	12p	0.267(5)	0.074(5)	0.0
S4	6l	0.160(6)	0.080(3)	0.0
S5	6m	0.586(2)	0.172(4)	0.5

*The letters $c, f, h, i, j, l, m, n, o, p,$ and r correspond to the Wyckoff notations.

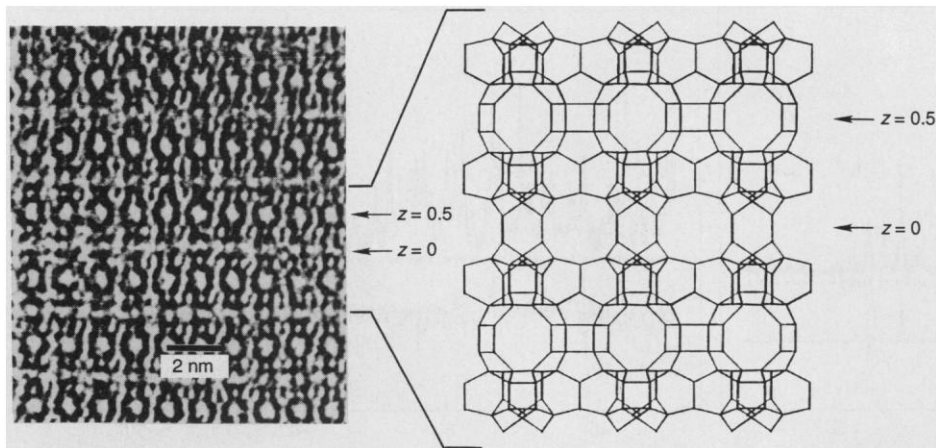


Fig. 2. An HREM lattice image of the $h0l$ MCM-22 projection, compared with the model structure. For clarity, the framework drawing is displayed at a larger scale than the micrograph; only T atoms are shown.

straint of these angles to linearity may be eliminated by removing the threefold symmetry imposed on this chain by the hexagonal crystal system and reducing the space group symmetry of the topology to $Cmmm$ (D_{2h}^{19} , no. 65). The DLS refinement of the MCM-22 model in this orthorhombic space group produced more reasonable T-O-T angles of 157° and 161° , respectively (Fig. 5). The unit cell parameters (based on a transformation of the hexagonal parameters) and the final atomic coordinates of this refinement are given in Table 2. A Rietveld refinement of the $Cmmm$ model was unsuccessful, however, possibly because the structure is too complex for the amount of available x-ray diffraction data.

Associated with all 10-ring windows is

scattering matter of unknown identity, some of which may be sodium cations that are present for charge balance; the rest may be detrital material that was introduced by calcination. This scattering matter is distributed over five different sites, each with partial occupancy. Sites S1 through S4, which are associated with the supercage, occur at distances ranging from 3.7 to 4.3 Å from framework oxygen atoms. Site S5 sits in the pocket of the folded 10-ring associated with the intralayer sinusoidal channels and is 3.8 to 4.1 Å from the oxygen atoms of that ring.

During the process of determining the structure of MCM-22, we also carefully considered other framework connectivities. None, however, produced the degree of

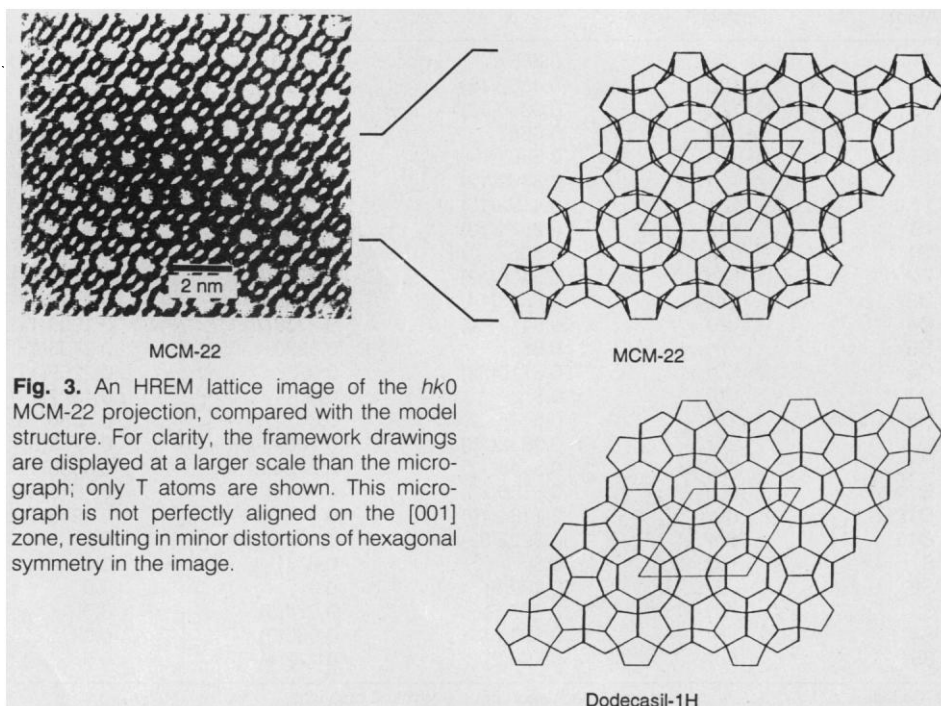


Fig. 3. An HREM lattice image of the $hk0$ MCM-22 projection, compared with the model structure. For clarity, the framework drawings are displayed at a larger scale than the micrograph; only T atoms are shown. This micrograph is not perfectly aligned on the $[001]$ zone, resulting in minor distortions of hexagonal symmetry in the image.

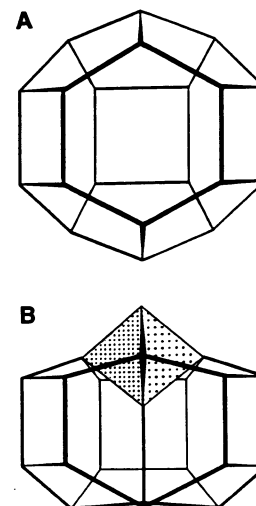


Fig. 4. (A) The $[4^3 5^6 6^3]$ cage in DOH, with idealized D_{3h} symmetry. (B) The $\{4^3 5^6 6^3 [4^3]\}$ cage in MCM-22, with idealized C_{3v} symmetry.

Table 2. Fractional atomic coordinates for MCM-22 based on DLS refinement in orthorhombic crystal system [space group $Cmmm$ (no. 65), $a = 24.4470$ Å, $b = 14.1145$ Å, $c = 24.8822$ Å].

Atom	Position*	x	y	z
T1	8o	0.3414	0.0	0.0625
T2	8o	0.2353	0.0	0.1248
T3	8o	0.3247	0.0	0.2136
T4	8o	0.3210	0.0	0.3398
T5	16r	0.1976	0.1904	0.1590
T6	16r	0.1182	0.3524	0.1443
T7	8n	0.0	0.3914	0.1728
T8	8o	0.1980	0.0	0.3506
T9	16r	0.1969	0.1915	0.2847
T10	16r	0.1125	0.3140	0.3441
T11	8n	0.0	0.3912	0.3000
T12	8o	0.1051	0.0	0.4380
T13	16r	0.0623	0.2043	0.4383
O1	4g	0.3543	0.0	0.0
O2	8o	0.2765	0.0	0.0744
O3	16r	0.3671	0.0931	0.0899
O4	8o	0.2684	0.0	0.1804
O5	16r	0.3593	0.0928	0.1965
O6	8o	0.3118	0.0	0.2763
O7	8o	0.2616	0.0	0.3692
O8	16r	0.3534	0.0927	0.3587
O9	16r	0.1970	0.0930	0.1244
O10	8m	0.25	0.25	0.1397
O11	16r	0.1431	0.2470	0.1433
O12	16r	0.0531	0.3398	0.1486
O13	4l	0.0	0.5	0.1531
O14	16r	0.2004	0.1695	0.2217
O15	8n	0.0	0.3850	0.2363
O16	16r	0.1890	0.0934	0.3157
O17	8m	0.25	0.25	0.3040
O18	16r	0.1437	0.2554	0.2979
O19	16r	0.0532	0.3401	0.3229
O20	4l	0.0	0.5	0.3195
O21	8o	0.1589	0.0	0.4017
O22	16r	0.1057	0.2539	0.3988
O23	16r	0.0677	0.0921	0.4278
O24	8n	0.0	0.2361	0.4254
O25	4h	0.1239	0.0	0.5
O26	8q	0.0764	0.2277	0.5

*The letters $g, h, l, m, n, o, q,$ and r correspond to the Wyckoff notations.

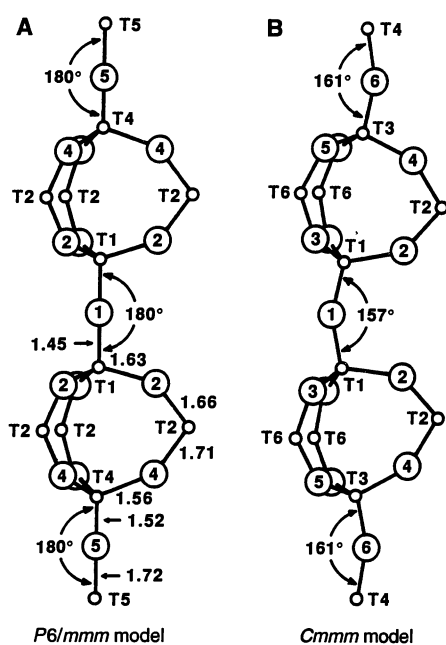


Fig. 5. Dimeric chain of T-O-[4³]-O-[4³]-O-T in MCM-22. **(A)** Bond lengths and angles derived from the Rietveld refinement in space group *P6/mmm*. **(B)** Bond angles derived from the DLS refinement in space group *Cmmm*.

agreement with observed XRD data that was obtained with this model. Despite its unusual topology, the framework connectivity for MCM-22 proposed here yields the best agreement with observed data. The discrepancy indices for the refinement are not unreasonable and are comparable with those (9) of other framework materials determined from powder XRD data.

The structure of MCM-22 may allow for a variety of applications in the petrochemical and refining industries. For example, MCM-22 may find applications in the catalysis of carbenium ion-mediated reactions, particularly those where the reactant size or the structure of the transition state intermediate is affected by the steric constraints presented by this zeolite.

REFERENCES AND NOTES

1. M. K. Rubin and P. Chu, U.S. patent 4,954,325 (1990) (assignee: Mobil Oil Corporation).
2. The chemical composition (in weight percent) of this product was determined to be N, 1.67; Na, 1.0; B, 1.06; Al₂O₃, 0.37; and SiO₂, 76.5. The molar ratios were SiO₂/Al₂O₃, 351; SiO₂/B₂O₃, 26.0; and SiO₂/(Al+B)₂O₃, 24.2.
3. A portion of the calcined, hydrated sample was placed in a flat plate and bathed in an 8 mm by 1 mm beam of 1.5371 Å radiation. A Si(111) single-reflection incident-beam monochromator and a Ge(220) analyzer crystal were used. The sample was scanned from 2θ = 3° to 75° in steps of 0.02° with a count time of 8 s per step. The instrument design at X7A uses a nonfocusing diffractometer geometry, so the ω-angle could be rocked during the data collection to reduce preferred-orientation effects that might be present in the sample.
4. Precise values for the unit cell parameters of the calcined material were determined during the

Rietveld refinement of the structure. The numbers in parentheses correspond to the standard error in the last digits.

5. Ch. Baerlocher, A. Hepp, W. M. Meier, DLS-76: A Program for the Simulation of Crystal Structures by Geometric Refinement (Institute of Crystallography and Petrography, ETH, Zurich, Switzerland, 1978).
6. Trial models for the MCM-22 framework were constructed with structural fragments deduced from *hk0* and *h0l* HREM lattice images (10). These fragments were interconnected to form frameworks satisfying the requirements of tetrahedral network bonding and the crystal symmetry of MCM-22, as determined from ED patterns and the indexing of the experimental XRD pattern. Calculated XRD patterns (11) for the models were computed from DLS-refined (5, 12) atomic coordinates. The framework model whose computed XRD powder pattern corresponded most closely to the experimental pattern has a maximum topological symmetry of *P6̄/mmm* (*D*_{6h}¹⁹, no. 191) (13). This model, which produced very low DLS figures-of-merit (14) *R* = 0.0020 and *σ* = 0.0083, served as the starting point for least squares refinements of the framework versus the experimentally observed XRD pattern by means of the Rietveld procedure (15), as implemented in the Generalized Structure Analysis System (GSAS) computer program package (16) from Los Alamos National Laboratory. Because of the complexity of the MCM-22 structure and the limited extent of diffracted intensities in the XRD pattern, soft constraints were imposed on interatomic distances during the structure refinement. In particular, T-O distances were specified as 1.61 Å and O-O distances were set to 2.63 Å, in line with idealized silicate geometry about the tetrahedral centers. Distances between adjacent tetrahedral centers were not constrained. Preliminary Rietveld refinement of the DLS-optimized framework with the synchrotron data reduced the discrepancy index *R*_p to ~0.30 after adjustment of the scale, profile, and lattice parameters. A difference Fourier synthesis computed at this point revealed the presence of nonframework atoms in the structure. Addition of these atoms to the calculated powder pattern and refinement of the soft-constrained framework coordinates resulted in a converged refinement with discrepancy indices *R*_p = 0.16, *R*_{wp} = 0.19, and *R*(*F*²) = 0.13. Sixty independent parameters were varied in the refinement, including 46 atom coordinates; 517 reflections were used, along with 76 soft constraints.

7. H. Gerke and H. Gies, *Z. Kristallogr.* **166**, 11 (1984).
8. A cage may be described by the rings of (Si,B)-O from which it is constructed, that is the number of T atoms (A, B, C, ...) in each ring and the total number of each type of ring (*u*, *v*, *w*, ...). This description may be represented by the symbol [*A^uB^vC^w*...]. For example, [4²5⁸10²] describes a cage consisting of two 4-rings (rings of 4 T atoms), eight 5-rings, and two 10-rings.
9. L. McCusker, *J. Appl. Crystallogr.* **21**, 305 (1988); E. B. Keller, W. M. Meier, R. M. Kirchner, *Solid State Ionics* **43**, 93 (1990); J. M. Bennett and R. M. Kirchner, *Zeolites* **11**, 502 (1991).
10. Images obtained on a Jeol 4000EX transmission electron microscope (TEM) at the high-resolution electron microscopy facility in the Center for Solid State Science at Arizona State University. The instrument was operated at 400 kV with a top-entry goniometer and has an interpretable resolution of ~1.6 Å at Scherzer defocus. Samples were prepared for study in the TEM by ultramicrotomy.
11. POWD10; D. K. Smith, M. C. Nichols, M. E. Zolensky, College of Earth and Mineral Sciences, Pennsylvania State University, University Park, PA (March 1983).
12. In these refinements, the prescribed T-O, O...O, and T...T distances (where T is a tetrahedrally coordinated atom, either Si or B in this case) were optimized at 1.61, 2.63, and 3.07 Å, respectively, with relative weights of 2.0, 1.0, and 0.1. The lattice parameters were allowed to refine. Both *R* and *σ* have been defined elsewhere (17). According to Gramlich-Meier, DLS refinements that are based on the weighting scheme used here and that produce residuals (*R*) less than 0.003 can be considered as realistic models (14).
13. T. Hahn, Ed., *Space-Group Symmetry*, vol. A of International Tables for Crystallography (Reidel, Dordrecht, 1983).
14. R. Gramlich-Meier, *Z. Kristallogr.* **177**, 237 (1986).
15. H. M. Rietveld, *J. Appl. Crystallogr.* **2**, 65 (1969).
16. A. C. Larson and R. B. Von Dreele, GSAS, Generalized Structure Analysis System (MS-H805, Los Alamos Neutron Scattering Center, Los Alamos National Laboratory, Los Alamos, NM, 1988).
17. S. L. Lawton and W. J. Rohrbough, *Science* **247**, 1319 (1990).
18. We thank P. A. Labun for technical assistance in obtaining the high-resolution electron micrographs.

11 March 1994; accepted 10 May 1994

Time-Resolved Imaging of Translucent Droplets in Highly Scattering Turbid Media

R. R. Alfano,* X. Liang, L. Wang, P. P. Ho

The spatial distribution of small translucent droplets inside a 50-millimeter-thick Intralipid solution was imaged with a picosecond time and spatial-gated Kerr-Fourier imaging system at a signal level of about 10⁻¹⁰ of the incident illumination intensity.

Early ballistic and snake light imaging (1-9) offers a nondestructive and noninvasive method to observe translucent ob-

Institute for Ultrafast Spectroscopy and Lasers, Mediphotonics Laboratory, New York State Center of Advanced Technology for Ultrafast Photonic Materials & Applications, Departments of Physics and Electrical Engineering, The City College and The Graduate School of The City University of New York, New York, NY 10031, USA.

*To whom correspondence should be addressed.

jects inside a highly scattering environment. With recent advances in the development of ultrafast lasers and ultrasensitive photodetectors, submillimeter spatial resolution of optical images has been achieved from both opaque (1, 3, 4) and translucent (8-10) phantoms in modeled turbid media. We report on two-dimensional imaging of translucent droplets; that is, we resolved phantoms without container boundaries and with different